JACS
JOURNAL OF THE AMERICAN CHEMICAL SOCIETY
Article
pubs.acs.org/JACS

Monitoring Molecular Mass Transfer in Cation-Free Nanoporous Host Crystals of Type AlPO-LTA

Florian Hibbe,[†] Jürgen Caro,[‡] Christian Chmelik,[†] Aisheng Huang,[‡] Tom Kirchner,[†] Douglas Ruthven,[§] Rustem Valiullin,[†] and Jörg Kärger*[,†]

[†]Department of Interface Physics, University of Leipzig, Linnéstraße 5, 04103 Leipzig, Germany
[‡]Institute of Physical Chemistry and Electrochemistry, Leibniz University Hannover, Callinstraße 3-3A, 30167 Hannover, Germany
[§]Department of Chemical Engineering, University of Maine, Orono, Maine 04469, United States

Supporting Information

ABSTRACT: Micro-imaging is employed to monitor the evolution of intra-crystalline guest profiles during molecular adsorption and desorption in cation-free zeolites AlPO-LTA. The measurements are shown to provide direct evidence on the rate of intra-crystalline diffusion and surface permeation and their inter-relation. Complemented by PFG NMR and integral IR measurements, a comprehensive overview of the diffusivities of light hydrocarbons in this important type of host materials is provided.

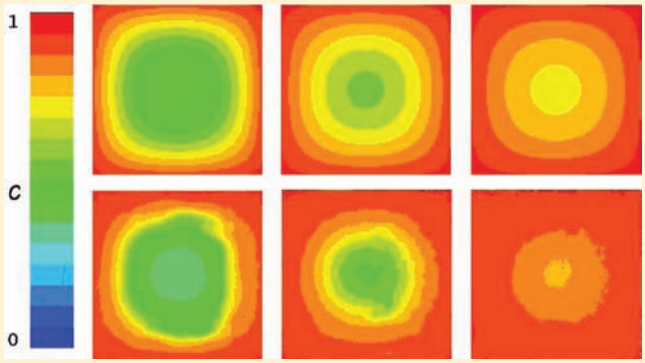

INTRODUCTION

It is well known that, under process conditions, the performance of nanoporous catalysts and adsorbents is often determined by mass transfer resistance. The introduction of pulsed field gradient (PFG) NMR to zeolite science and technology[1,2] permitted the first direct measurement of molecular diffusion in the interior of the individual crystallites. The primary quantity accessible by this type of measurement is the probability distribution of the diffusion path lengths within the sample and, thus, of the mean-square displacement $\langle r^2(t)\rangle$ of the guest molecules on their diffusion path during an observation time t (typically a few milliseconds).[3−5] In this way, with root-mean-square displacements $\langle r^2(t)\rangle^{1/2}$ sufficiently small in comparison with crystal sizes, the intra-crystalline self-diffusivity D^* may be easily determined by the Einstein relation,

$$\langle r^2(t)\rangle = 6D^*t \qquad (1)$$

Equation 1 is completely equivalent to the definition of the self- (or tracer) diffusivity D^* by Fick's first law as the factor of proportionality between the flux of labeled molecules and their concentration gradient, under the conditions of a uniform total concentration.[1,5]

Operating under equilibrium conditions and with assemblages of crystals, PFG NMR is unable to record mass transfer in the interior of a particular, individual crystal. Although NMR tomography has proved to be useful for recording guest concentrations and fluxes in beds of crystals,[6] despite substantial methodological progress,[7,8] spatial and temporal resolutions are not yet high enough to record mass transfer in the interior of the individual crystallites. With the successful application of interference microscopy (IFM)[9,10] and infrared microscopy (IRM)[11,12] to micro-imaging with individual crystals,[13,14] however, this type of information has now become accessible.

The physical quantity measured by these techniques is the integral (in the observation direction) of the guest concentration rather than the concentration itself. Diffusion studies exploiting these techniques have therefore been performed primarily with host systems containing one- and two-dimensional (1D and 2D) channel systems[15] where, by observation perpendicular to the channel direction, the concentration in the observation direction is constant and, thus, directly accessible. However, most nanoporous materials have three-dimensional (3D) pore systems which provide much better conditions for fast mass exchange between the host interior and the surrounding fluid, a critical requirement for many technological applications. The first diffusion studies by micro-imaging with 3D pore systems, notably with zeolites of types MFI[10] and SAV,[16] were additionally complicated by the fact that, as a consequence of host anisotropy, flux rates through the different crystal faces were very different.

Much better conditions for diffusion studies with 3D pore networks should therefore be provided by host systems of cubic symmetry. In this context, zeolites of structure type LTA (with

Received: December 8, 2011
Published: April 17, 2012

   dx.doi.org/10.1021/ja211492b | J. Am. Chem. Soc. 2012, 134, 7725−7732

NaCaA being the most important representative) appear to be ideal candidates for such studies. They are available as cubes with edge lengths of up to tens of micrometers[17] and are widely used in many important processes in the petrochemical industry.[18] Probably as a consequence of the bivalent cations, however, under the experimental conditions of micro-imaging with individual NaCaA-type zeolites[9] it was impossible, so far, to attain fully reversible adsorption−desorption cycles. With the advent of cation-free zeolites of type LTA made of SiO_2 (ITQ-29)[19] or $AlPO_4$,[20,21] this problem can now be circumvented.

In addition to their relevance for fundamental diffusion studies, zeolites of type LTA are of particular technological relevance. Together with further zeolite structure types (CHA, ERI, DDR[22]), they constitute the important class of "small-pore" zeolites, the pores of which are constricted by eight-membered oxygen rings. When not obstructed by cations, their free apertures assume well-defined values between 3.5 and 4.5 Å, making them ideal host systems for shape-selective separation of smaller molecules.

We report here the results of an in-depth study of mass transfer in cation-free zeolites of type LTA with propylene as the guest molecule. Propylene shows particularly advantageous conditions for pore space probing by IFM, allowing the determination of both the intra-crystalline (transport) diffusivities and surface permeabilities, as a function of loading, with unprecedented accuracy. The data so obtained are compared with the results of complementary studies, involving both other microscopic techniques of diffusion measurements (IRM and PFG NMR) and other guest molecules (ethane and propane).

EXPERIMENTAL SECTION

Measuring Techniques. A detailed description of the measuring techniques applied may be found in recent reviews[23,14] and the monograph.[5] We therefore present here only a brief summary of the fundamental principles and limitations of the techniques. All the techniques applied in this study are referred to as "microscopic" since they are able to record directly molecular transport over distances that are small in comparison with the dimensions of the crystals under study.

The present study was focused on the application of IFM. This technique records differences in the optical path lengths of light beams through the crystal with those passing through the surroundings. Since the optical density of the crystal is a function of the guest loading, the information thus obtained may be converted into the integral

$$c(x, y, t) = \int_0^L c(x, y, z, t)\, dz \tag{2}$$

over the guest concentration $c(x,y,z,t)$ in the observation direction (assigned to the direction of the z coordinate), with L denoting the crystal thickness in this direction. With propylene as the guest molecule, variation in the concentration integrals during molecular uptake or release could be recorded with pressure steps sufficiently small that the intra-crystalline (transport) diffusivity could be assumed to be constant and uniform during each transient sorption experiment. For each individual pressure step the intra-crystalline diffusivity (D) and the surface permeability (α) were determined by searching for the best fit of the concentration integrals calculated from the solution of the diffusion equation (Fick's second law)

$$\frac{\partial c}{\partial t} = D\left(\frac{\partial^2 c}{\partial x^2} + \frac{\partial^2 c}{\partial y^2} + \frac{\partial^2 c}{\partial z^2}\right) \tag{3}$$

to the experimentally determined values.[24] The transport diffusivity (defined by Fick's first law as the factor of proportionality between flux and the concentration gradient) and the surface permeability (appearing in the boundary condition of the diffusion equation as the ratio between the flux through the crystal surface and the difference between the actual surface concentration and the concentration in equilibrium with the external guest pressure) are considered as free parameters.

The IFM measurements were carried out using the interference microscope Jenamap p dyn (Carl Zeiss GmbH) controlled by a personal computer, a CCD camera (SenSys KAF 0400, Photometrics), and a vacuum system.[9,25] The attainable resolutions in time and space (i.e., in the $x-y$ plane, perpendicular to the direction of observation) were about 15 s and 0.5 μm, respectively.

Diffusion measurements by IRM were also performed by following the response of the host system following a variation of the guest pressure in the surrounding atmosphere. If analyzed by a focal plane array detector, IRM also provides the concentration integral, eq 2, as the primary experimental quantity. Complications result, however, because the observation beam deviates by about 15° from the vertical and, with values of about 3 μm, the spatial resolution is significantly inferior to IFM.[12] Therefore, in the present study, IRM was applied exclusively in the integral mode. In this case, IRM records the total uptake of the selected crystal. In comparison with IFM, in this way a notably better time resolution (fractions of seconds) is attained. Moreover, operating with a single crystallite and, hence, with an extremely large surface-to-volume ratio, disturbing effects due to the finite rate of heat release (which is known to corrupt diffusion measurement with fast uptake and release in macroscopic sample arrangements[5,26]) may be excluded.[27]

In contrast to IFM and IRM, measurements by PFG NMR are performed under equilibrium conditions, with the mean-square displacement (eq 1) of the guest molecules as the key quantity. PFG NMR measurements are based on the same fundamental law which is also exploited in NMR tomography[7,8] (which today, generally referred to as MRT,[28] has become the most powerful imaging technique in medical diagnosis), namely proportionality between the intensity of the magnetic field and the nuclear magnetic resonance frequency. In this way, by superimposing a constant magnetic field an inhomogeneous one (the "field gradient"), the spectrum shows the spin distribution in the gradient direction. In PFG NMR, by the application of field gradients (of amplitude g) over two short intervals (of duration δ) at separation t (the "observation time"), one is able to determine the probability distribution of molecular shifts during t (i.e., the difference in the locations of the diffusing molecules between the first and second field gradient pulses). The experimentally observable quantity is the intensity of the so-called NMR spin echo, i.e., of a signal which may be generated by an appropriately chosen sequence of radio-frequency pulses.[29] Under the influence of the field gradient pulses, the spin−echo may be shown[3,23,14] to be attenuated by the factor

$$\psi(\gamma\delta g, t) = \exp(-\gamma^2\delta^2 g^2 \langle z(t)^2\rangle/2) \tag{4}$$

with $\langle z(t)^2\rangle$ denoting the mean-square displacement of the molecules under study in the direction of the field gradient pulses applied. With eq 1 and assuming isotropy, eq 4 may be written in the form

$$\psi(\gamma\delta g, t) = \exp(-\gamma^2\delta^2 g^2 D^* t) \tag{5}$$

As a necessary and sufficient requirement of the validity of eqs 4 and 5, the diffusion behavior of the majority of the guest molecules under study must undergo ordinary diffusion (subject to Fick's second law, eq 3) in a quasi-infinitely extended homogeneous space.

Referring to different physical situations, the coefficients of transport diffusion and self-diffusion cannot be expected to coincide. In general, they are interrelated by an equation of the type[30,31]

$$1/D^* = 1/D_0 + \theta/Đ_{AA} \tag{6}$$

D_0 is the (thermodynamically) corrected (transport) diffusivity which is correlated with the transport diffusivity via the relation

$$D = D_0 \partial \ln p/\partial \ln c \tag{7}$$

dx.doi.org/10.1021/ja211492b | J. Am. Chem. Soc. 2012, 134, 7725−7732

with $\partial \ln p/\partial \ln c$ denoting the "thermodynamic factor", i.e., an extra driving force of the diffusion flux resulting from non-ideality, i.e., from deviations from linearity in the adsorption isotherm $c(p)$.[5] $Đ_{AA}$, referred to as the mutual Stefan–Maxwell diffusivity,[32,30,31] is a measure of the mutual "friction" of the guest molecules (as opposed to their friction with the lattice, which is captured by D_0).

For the host–guest systems under study, the limiting step of guest diffusion is known to be the passage through the windows between adjacent cages. Hence, the second term on the right-hand side of eq 6 is easily seen to be negligibly small so that, by combining eqs 6 and 7, the self-diffusivity is seen to coincide with the corrected diffusivity. One arrives at exactly the same result by application of the absolute rate theory, i.e., by considering the passage through one window as the "activated" state during molecular propagation.[5] Considering short-chain-length hydrocarbons in MOF ZIF-8, essentially this situation may be assumed to occur,[33] and, correspondingly, the above conclusions were found to be perfectly confirmed by comparative measurements of self-diffusion and transport diffusion.[12] It is for this reason that, in the Results and Discussion section, the PFG NMR self-diffusivities are compared with the corrected transport diffusivities from the micro-imaging experiments.

Material. The AlPO-LTA single crystals were prepared according to the procedure reported in ref 21 using the crown ether Kryptofix 222 as structuring agent, which was first proposed by Schreyeck et al.

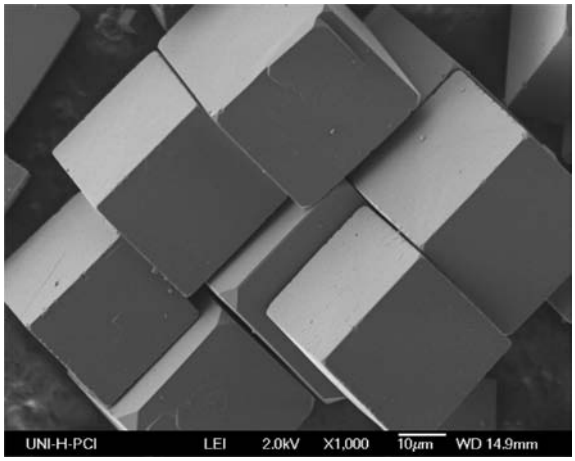

Figure 1. SEM image of the AlPO-LTA single crystals used in this study.

The habit of the thus-produced crystals is shown in Figure 1. Prior to the diffusion studies, the as-made AlPO-LTA single crystals were calcined over a time span of 6 h at 573 K in O_3/air (with about 100 ppm of O_3 in air), for removing the template Kryptofix 222 used during synthesis, with heating and cooling rates of 0.2 K/min.

This sophisticated de-templation process using an air/ozone mixture had to be developed and applied in order (i) to avoid cracking of the big single crystals shown in Figure 1 and (ii) to remove residual C deposition as found after common calcination in air (see Supporting Information).

RESULTS AND DISCUSSION

Propylene Diffusion in AlPO-LTA Single Crystals. Figure 2a gives an overview of the IFM experiments performed with propylene in AlPO-LTA single crystals: In a first series, the propylene pressure was increased in small steps up to a maximum pressure of 600 mbar. After each pressure step, the evolution of the intra-crystalline particle concentration was recorded until equilibrium was established. Desorption, initiated by a stepwise decrease in the surrounding pressure, was recorded correspondingly (beginning at 250 mbar). In

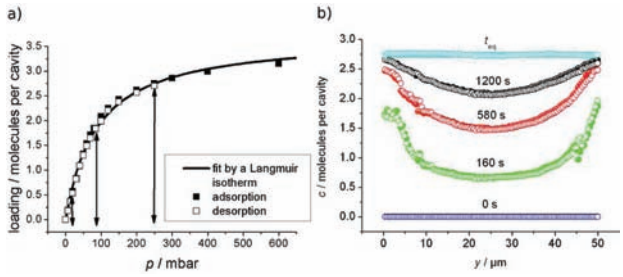

Figure 2. Overview of the IFM experiments with propylene in AlPO-LTA crystals at 295 K. (a) The loadings measured in the stepwise adsorption and desorption experiments are found to be in good agreement with each other and with the results obtained with larger pressure steps (0–20–0 mbar, 0–100–0 mbar, 0–250–0 mbar, arrows in the representation). They are well approximated by a Langmuir isotherm (full line). (b) Concentration profiles recorded by IFM through the crystal center (i.e., profiles along the central horizontal and vertical lines in the 2D plots as shown in Figure 4) during two subsequent sorption experiments (open and filled symbols) with a pressure step from 0 to 250 mbar, exemplifying the reproducibility of the measurements.

addition, also a few ad- and desorption experiments with large pressure steps (arrows in Figure 2a) were performed. The equilibrium loading was shown to be the same in both sets of experiments. In contrast to the behavior observed with cation-containing LTA,[9,34] molecular uptake and release with one and the same crystal was found to be completely reproducible after an adsorption–desorption cycle, as exemplified by Figure 2b.

The transport parameters, i.e., the intra-crystalline transport diffusivity D and the surface permeability α, are obtained by considering the concentrations resulting from the solution of the diffusion equation for uptake by a cube of the extension $(2l)^3$

$$\frac{c(x_1, x_2, x_3, t)}{c(t=\infty)} = 1 - \sum_{n_{x_i}=1}^{\infty} \prod_{i=1}^{3} \frac{2L \exp(-\beta_{n_{x_i}} Dt/l^2) \cos\left(\beta_{n_{x_i}}\left(\frac{x_i - l}{l}\right)\right)}{(\beta_{n_{x_i}}{}^2 + B^2 + B)\cos(\beta_{n_{x_i}})} \quad (8)$$

where β_n is the nth root of $\beta \tan(\beta) = B = l\alpha/D$.

The diffusivity and the surface permeability were varied to yield the best fit between the integrals of the calculated concentrations and those measured by IFM. The individual pressure steps considered for these studies were small enough so that, during each individual uptake (or release) experiment, both the diffusivity and the surface permeability may be assumed to be constant, as implied by eq 8. Figure 3 shows the resulting data.

It is remarkable that both transport diffusivities and surface permeabilities are found to vary with concentration in exactly the same way over more than an order of magnitude. This pattern of behavior was recently observed for short-chain alkanes in MOF Zn(tbip).[35] This observation has given rise to a new picture of the nature of transport resistances on the surface of nanoporous materials, since it suggests that the resistance is caused by an essentially impenetrable wall with dispersed "holes" rather than by a quasi-homogeneous layer of dramatically reduced permeability.[36] Since the MOFs of type Zn(tbip) consist of parallel chains of cages,[37] it must also be assumed that, within the real structure of the Zn(tbip) crystals

dx.doi.org/10.1021/ja211492b | J. Am. Chem. Soc. 2012, 134, 7725–7732

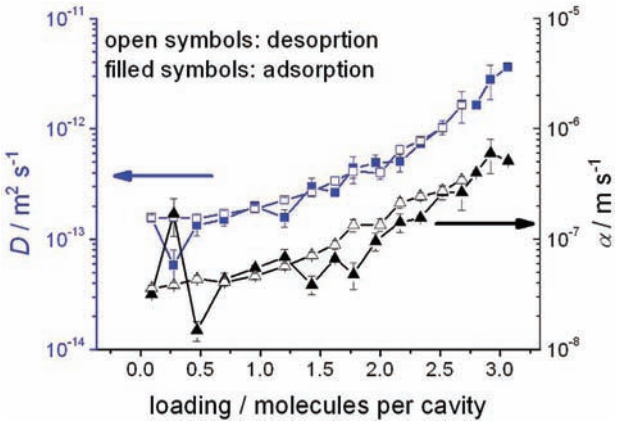

Figure 3. Transport diffusivities D (squares) and surface permeabilities α (triangles) of propylene in AlPO-LTA at 295 K, calculated from the transient concentration profiles recorded by IFM during molecular uptake following stepwise pressure change.

under study, there must be defects that allow mass transfer between different chains of cavities. The observation that this same pattern of diffusion and permeation behavior is observed in the 3D pore structure of AlPO-LTA is therefore important because, in this system, there is no need for any further structural assumptions, and one may refer directly to the classical relation of the effective medium approach,[38,38,39] where the permeability through an impermeable boundary with, e.g., permeable circular holes of diameter d and separation L, is given by the relation

$$\alpha = d/L^2 \times D \tag{9}$$

which may be rearranged to

$$\frac{\alpha}{D} d \approx p_{\text{open}} \tag{10}$$

yielding a rule of thumb for an estimate of the fraction p_{open} of unblocked surface area.

The increase of this fraction, for a fixed permeability-to-diffusivity ratio, with increasing hole diameter is a direct consequence of eq 9 and may easily be rationalized by realizing that, for a given value of p_{open}, the efficiency of the openings for mass transfer increases with their degree of dispersion.

With $\alpha/D \approx 2 \times 10^5$ m^{-1} as resulting from our experiments (Figure 3) and with $d \approx 1.2$ nm corresponding to the highest degree of hole dispersion (the limiting case in which, on the external surface, unblocked windows do not occur in adjacent unit cells), p_{open} is found, from eq 10, to be of the order of 10^{-4}. This means that, among several 1000 "windows" connecting the intra-crystalline space with the surroundings, only a single one is permeable. Equation 10 further indicates that, for the given permeation-to-diffusion ratio, the percentage of unblocked windows, p_{open}, will become larger when there is some "clustering" of the unblocked windows on the crystal surface.

By comparison of the respective time constants ("first moments"[5,40]) of molecular uptake and release under diffusion ($\tau_D \approx R^2/(15D)$) and barrier ($\tau_\alpha \approx R/(3\alpha)$) control, with the above-given permeability–diffusivity ratio $\alpha/D \approx 2 \times 10^5$ m^{-1} and a mean crystal radius $R \geq 20$ μm, the diffusion resistance is found to exceed the surface resistance by 1 order of magnitude. It is important to note that, being based on the direct measurement of molecular fluxes and their local distribution, micro-imaging is able to provide accurate quantitative data on surface permeabilities, even under these conditions under which any of the conventional techniques, based on either an analysis of the shape of the uptake/release curves or (as in the fast NMR tracer desorption technique[41]) a comparison of uptake/release with intra-crystalline diffusivities, would not be applicable.

Comparative Diffusion Studies of Light Hydrocarbons in AlPO-LTA. Figure 4 provides examples of the complete

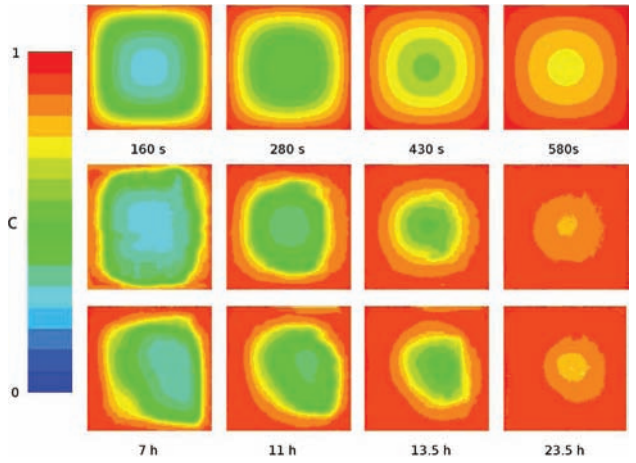

Figure 4. IFM profiles of the concentration integrals perpendicular to a crystal face during three-dimensional uptake of propylene (middle) and propane (bottom) in one and the same crystal of AlPO-LTA after a pressure step from 0 to 250 mbar at 295 K and their representation for an ideal cubic structure (top), following the analytical expressions of intra-crystalline concentration (eq 8) determined by assuming constant surface permeability (2×10^{-7} m s^{-1}) and intra-crystalline diffusivity (3×10^{-13} m^2 s^{-1}).

information provided by IFM, namely the 2D representation of the evolution of the concentration integrals over a crystal face. It simultaneously illustrates the particularly convenient measuring conditions provided by propylene as a guest molecule. The analytical results, as obtained by integration over eq 8 with an ideally cubic crystal, are also provided, where constant values for both the diffusivity (3×10^{-13} m^2 s^{-1}) and surface permeability (2×10^{-7} m s^{-1}) have been assumed. These values were chosen to demonstrate the close agreement between the theoretically predicted and experimentally observed concentration patterns. Small differences between the measured and simulated profiles can be attributed to the simplifying use of constant diffusivity and permeability values in the simulations as well as to possible deviations from crystal regularity and to the noise inherent to all experimental measurements. The last two reasons also explain the small deviations in the measured profiles from ideal symmetry.

The comparison between propane and propylene yields two important differences. While the time scale of transient sorption experiments with propylene (minutes) is ideally suited for the performance of the experiments (as presented in greater detail in the previous section), time spans over days, as required for the experiments with propane, make the measurements more difficult. For propane, we have therefore confined ourselves to the single measured point shown in Figure 6b.

As another remarkable difference, the concentration profiles recorded during propane adsorption are found to deviate much more strongly from symmetry than those obtained with propylene on one and the same crystal. These deviations are

dx.doi.org/10.1021/ja211492b | J. Am. Chem. Soc. 2012, 134, 7725–7732

particularly pronounced during the initial stage of uptake, when the influence of the surface resistances is particularly significant. It is most likely, therefore, that the assumption of a homogeneous surface permeability as implied in our analysis is less accurately fulfilled for propane. This explanation would nicely correspond with the fact that the critical diameter of propane is closer than that of propylene to the window diameter.

With ethane, on the other hand, the time scales of uptake and release dropped to seconds which, with our present experimental system, is too fast to allow monitoring by IFM micro-imaging. In this case, IR microscopy in the integral mode has therefore been applied, yielding the time dependence of the total molecular uptake on individual crystals. By inspecting the pronounced curvature of the concentration profiles[42] as well as by comparing the respective time constants (see above), for both propylene and propane, any dominance of surface resistance on the overall uptake on AlPO-LTA may be excluded. We therefore modeled the uptake of ethane as measured by IRM by the analytical solution for 3D, diffusion-controlled uptake by a cube of extension $(2l)$[3]

$$\frac{m(t)}{m(t=\infty)} = 1 - \frac{512}{\pi^6} \sum_{n_{x,y,z}=1}^{\infty} \frac{\exp\left(-\frac{\pi^2 Dt}{4l^2}\left((2n_x-1)^2+(2n_y-1)^2+(2n_z-1)^2\right)\right)}{(2n_x-1)^2(2n_y-1)^2(2n_z-1)^2} \quad (11)$$

The (apparent) intra-crystalline diffusivity as resulting from the best fit between the analytic expression and the experimental data was taken as an estimate of the intra-crystalline transport diffusivity. The corresponding corrected diffusivities (eq 7) are shown below in Figure 6b. Also included in Figure 6b are the results of IR measurements with propylene, following the same type of analysis. Their agreement with the data obtained by monitoring the intra-crystalline concentration profiles nicely confirms the validity of our approach.

The high mobility which prohibits the observation of transient intra-crystalline concentration profiles for ethane in AlPO-LTA makes it a most suitable system for PFG NMR measurements of intra-crystalline self-diffusion.[43] The PFG NMR signal attenuation could be followed over almost 2 orders of magnitude, exhibiting a monoexponential decay. This is exactly the behavior which, following eqs 4 and 5, is to be expected for unperturbed intra-crystalline diffusion. Correspondingly, the resulting diffusivities were found to be unaffected by a variation of the observation time from 10 up to 200 ms. With the diffusivities shown in Figure 6b, via eq 1 the root-mean-square displacements of the diffusing guest molecules are found to vary from about 2 up to 10 μm.

Effect of Window Dimensions. The effect of the window dimensions on the diffusion of small molecules in 8-ring zeolites has been studied in some detail, especially for the CHA family.[44−46] The bond lengths of Al−O, P−O and Si−O are significantly different: Al−O = 1.75 Å, Si−O = 1.61 Å, P−O = 1.53 Å, 0.5(Al−O + P−O) = 1.64 Å.

As a result, the unit cell size and the window dimensions of the CHA structure can be adjusted by changing the Si/Al ratio or by introducing phosphorus into the lattice to form the AlPO or SAPO analogues (ALPO-34 or SAPO-34). The SAPO-34 sample considered here had a Si/P ratio of about 1.4, so the framework dimensions are closer to CHA than to ALPO-34. For the same reason, the dimensions of the 8-rings in LTA (Si/Al = 1.0) are somewhat larger than for the pure silica analogue ITQ-29. The 8-ring dimensions for some of the CHA and LTA structures, derived from accurate XRD measurements, are summarized in Table 1.[46]

Table 1. Window Dimensions (Å) for Modified CHA and Other 8-Ring Structures

CaA	4.6 × 4.2	AlPO-34	3.7 × 4.5
ITQ-29	4.2 × 4.0	SiCHA	3.7 × 4.2
CHA	3.9 × 4.1	DD3R	3.65 × 4.4
SAPO-34	3.8 × 4.3		

Figure 5 summarizes experimental diffusivity data for propylene, ethylene, and methane from several different

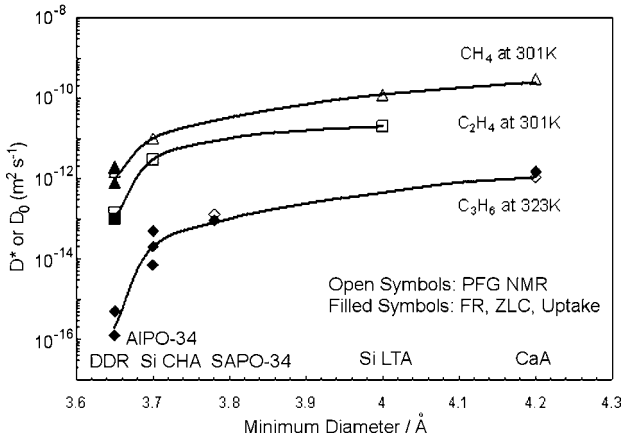

Figure 5. Correlation of diffusivity data for light hydrocarbons in 8-ring zeolites with minimum window diameter. Data are from refs 44−48.

sources. The diffusivities correlate closely with the minimum diameter of the 8-ring. It is clear that the variation is dramatic, spanning 3 orders of magnitude for propylene, with an especially sharp decline when the minimum ring diameter reaches the critical molecular diameter (~3.75 Å). A similarly dramatic drop in the diffusivities is known for cyclohexane in the 10-ring zeolites MFI where, on the other side, already a faint increase in the pore opening under liquid-phase adsorption leads to an enhancement of the diffusivities by several orders of magnitude.[5]

Similar effects are seen for the LTA structures, although since, for these structures, the minimum 8-ring diameters are somewhat larger, the variations in diffusivity are less dramatic. Figure 6 compares the results from the present study (Figure 6b) with previous diffusion measurements for the cation-containing zeolite NaCa LTA (Figure 6a) and for the pure silicon LTA analogue (ITQ-29, Figure 6c). Taking account of the difference in temperature, the data for propane and propylene in NaCaA (Figure 6a) are consistent with the earlier macroscopic (ZLC and tracer ZLC) measurements as well as with the earlier PFG NMR data,[50] which are not shown.

The data confirm the observation that guest diffusion in the cation-free LTA isomorphs[19] is notably slower than in CaA.[44,45] It is remarkable that, even for ethane, for which the critical diameter (3.7 Å) is substantially smaller than the free diameter of the 8-ring, there is an order of magnitude difference in diffusivity between CaA and ITQ-29. Hindrance of rotation in

dx.doi.org/10.1021/ja211492b | J. Am. Chem. Soc. 2012, 134, 7725−7732

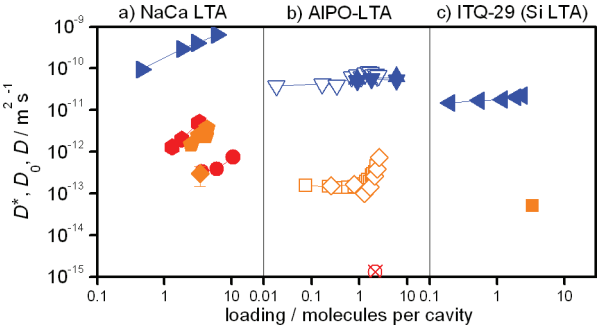

Figure 6. Diffusivities (full symbols, self-diffusivities; open symbols, corrected diffusivities) of ethane (triangles), propylene (squares and diamonds), and propane (circles) at room temperature (298 K) in different LTA-type zeolites determined by microscopic measuring techniques. (a) Na(75)CaA (NaCa LTA): PFG NMR self-diffusivities of ethane (▶),[49] propylene (◆),[44] and propane (●),[49] and ZLC/TZLC data for propane (⬢) and propylene (⬟) in CaA (~75% exchanged) at 358 K.[47] (b) AlPO-LTA (this study): PFG NMR self-diffusivities of ethane (▲,▼; two different specimens) and corrected (transport) diffusivities of ethane (∇), corrected (transport) diffusivities of propylene resulting from IFM (□) and IRM (◇), and transport diffusivity of propane (⊗). (c) ITQ-29 (Si LTA): PFG NMR self-diffusivities of ethane (◀)[44] and propylene (■).[45]

the transition state offers a possible explanation. In cationic LTA the effect of the window dimensions is complicated by the presence of bivalent calcium cations, which are known to reduce the diffusivity of the guest molecules especially for unsaturated species.[51] This probably explains the coincidence of the diffusivities for propane and propylene (which is slightly smaller) in CaA, as shown in Figure 6a. However, in the cation-free samples, the observed decrease in the diffusivities must clearly be ascribed to the reduction in the window dimensions. In conformity with this conclusion, the reduction of the diffusivity is most pronounced for propane, which has the largest critical diameter of all guest molecules considered.

Micro-imaging during uptake and release of propylene with carefully detemplated crystals of AlPO-LTA (see Figures 2b and 4) reveals transient concentration profiles in perfect agreement with the analytical expressions derived for perfect crystals, providing strong evidence that these processes are dominated by intra-crystalline diffusion. This is of particular importance since earlier PFG NMR diffusion studies with different batches of pure-silica LTA were found to lead to significant differences in diffusivity.[52] This was taken as an indication of the existence of additional intra-crystalline transport resistances[53] such as are known to occur, e.g., in zeolites of the MFI and FAU types.[54]

Temperature Dependence. MD simulations with ethane in pure-silica LTA[55] have suggested the rather spectacular option that, with increasing temperature, the guest diffusivity may decrease rather than increase. Such behavior can be rationalized by realizing that temperature increase also accelerates molecular rotation around the direction perpendicular to the molecule's longitudinal extension, which might hamper molecular passage through the tight windows. The temperature-dependent diffusivity measurements by PFG NMR shown in Figure 7, however, do not show any indication of such deviations from a normal Arrhenius pattern. The observed activation energy of +3.7 kJmol^{-1} is in remarkably good agreement with the NaCaA data.[51]

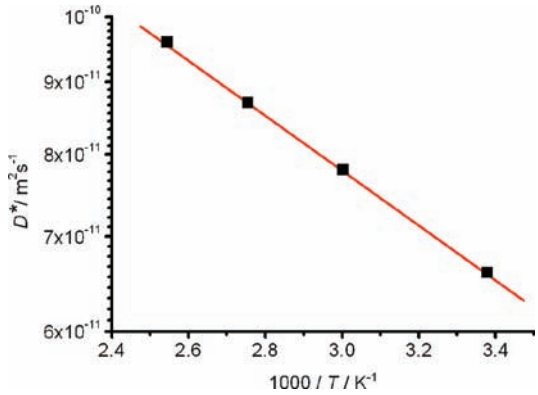

Figure 7. Arrhenius plot of the PFG NMR self-diffusivity of ethane in AlPO-LTA with a loading of about 6 molecules per cavity.

CONCLUSIONS

The synthesis of large crystals of cation-free zeolites of type AlPO-LTA with perfect crystal habit[21] has allowed, for the first time, detailed diffusion studies of nanoporous host materials with three-dimensional pore networks by micro-imaging. The cubic symmetry of the host material allows a hitherto unattained accuracy in the measurement of both the intra-crystalline diffusivities and surface permeabilities, as demonstrated in an in-depth study with propylene as a guest molecule.

Notably, over concentration ranges where both the surface permeability and intra-crystalline diffusivity varied over more than an order of magnitude, their mutual ratio was found to remain constant. Similar behavior was recently observed by Hibbe et al. for light hydrocarbons in Zn(tbip), which has a uni-dimensional pore structure.[35] These observations provide strong support for the view that, also for the AlPO-LTA crystals under study, under the given conditions of synthesis and sample activation prior to diffusion measurements, the surface resistance arises from complete blockage of most of the pore entrances rather than from the presence of a more or less uniform surface layer with a substantially reduced permeability.

By employing IR micro-imaging and PFG NMR as alternative, complementary "microscopic" techniques for diffusion measurement, our understanding of the behavior of AlPO-LTA was extended to guest molecules of both higher (ethane) and lower (propane) diffusivities. As a general feature of all these studies, the diffusivities of guest molecules in the cation-free LTA zeolites (ITQ-29 and AlPO-LTA) were found to be significantly smaller than in the cation-containing LTA-type zeolite NaCaA.[49] As originally pointed out by Hedin et al., this is consistent with the slight reduction of the window apertures of the Si and ALPO forms.[45]

Although the general features of the diffusional behavior of small molecules in type A zeolites have been reasonably well established from more traditional macroscopic measurements, the present study illustrates the remarkable level of detail that can be derived from the application of a combination of different microscopic techniques. In this context it is perhaps worth quoting the final sentence of Donald Breck's two 1956 papers reporting the synthesis and properties of Zeolite A, the first synthetic zeolite:[56] "This study of the Type A zeolite structure has maintained the interest of the authors because it has led to a logical correlation between structural features and adsorption phenomena."

The development and application of new approaches to the study of intra-crystalline diffusion have made this statement

dx.doi.org/10.1021/ja211492b | J. Am. Chem. Soc. 2012, 134, 7725−7732

relevant in ways that could scarcely have been imagined in 1956.

■ ASSOCIATED CONTENT

Supporting Information

Details on post-synthesis sample treatment and applied de-templation procedures. This material is available free of charge via the Internet at http://pubs.acs.org.

■ AUTHOR INFORMATION

Corresponding Author

kaerger@physik.uni-leipzig.de

Notes

The authors declare no competing financial interest.

■ ACKNOWLEDGMENTS

Financial support by the German Science Foundation (International Research Training Group "Diffusion in Porous Materials" and Package Application "Diffusion in Zeolites"), the Humboldt Foundation, and Fonds der Chemischen Industrie are gratefully acknowledged. Prof. Gesing (Hamburg) is thanked for XRD and TG/DSC.

■ REFERENCES

(1) Kärger, J.; Pfeifer, H. *Zeolites* **1987**, *7*, 90−107.
(2) Hong, U.; Kärger, J.; Pfeifer, H. *J. Am. Chem. Soc.* **1991**, *113*, 4812−4815.
(3) Price, W. S. *NMR Studies of Translational Motion*; University Press: Cambridge, 2009.
(4) Callaghan, P. T. *Translational Dynamics and Magnetic Resonance*; Oxford Univ. Press: Oxford, 2011.
(5) Kärger, J.; Ruthven, D. M.; Theodorou, D. N. *Diffusion in Nanporous Materials*; Wiley-VCH: Weinheim, 2012.
(6) (a) Sederman, A. J.; Gladden, L. F. *Chem. Eng. Sci.* **2001**, *56*, 2615−2628. (b) Bär, N. K.; Balcom, B. J.; Ruthven, D. M. *Ind. Eng. Chem. Res.* **2002**, *41*, 2320−2329.
(7) Gladden, L. F.; Mantle, M. D.; Sederman, A. J. In *Handbook of Heterogeneous Catalysis*, 2nd ed.; Ertl, G., Knözinger, H., Schüth, F., Weitkamp, J., Eds.; Wiley-VCH: Weinheim, 2008; Vol. *III*, pp 1784−1801.
(8) Lysova, A. A.; Koptyug, I. V. *Chem. Soc. Rev.* **2010**, *39*, 4585−4601.
(9) Schemmert, U.; Kärger, J.; Weitkamp, J. *Microporous Mesoporous Mater.* **1999**, *32*, 101−110.
(10) Kärger, J.; Kortunov, P.; Vasenkov, S.; Heinke, L.; Shah, D. B.; Rakoczy, R. A.; Traa, Y.; Weitkamp, J. *Angew. Chem., Int. Ed.* **2006**, *45*, 7846−7849.
(11) Chmelik, C. FTIR Microscopy as a Tool for Studying Molecular Transport in Zeolites. Ph.D. thesis, Leipzig University, 2007.
(12) Chmelik, C.; Bux, H.; Caro, J.; Heinke, L.; Hibbe, F.; Titze, T.; Kärger, J. *Phys. Rev. Lett.* **2010**, *104*, 85902.
(13) Weckhuysen, B. M. *Angew. Chem., Int. Ed.* **2009**, *48*, 4910−4943.
(14) Chmelik, C.; Kärger, J. *Chem. Soc. Rev.* **2010**, *39*, 4864−4884.
(15) (a) Heinke, L.; Kortunov, P.; Tzoulaki, D.; Kärger, J. *Phys. Rev. Lett.* **2007**, *99*, 228301. (b) Tzoulaki, D.; Heinke, L.; Li, J.; Lim, H.; Olson, D.; Caro, J.; Krishna, R.; Chmelik, C.; Kärger, J. *Angew. Chem., Int. Ed.* **2009**, *48*, 3525−3528.
(16) (a) Castro, M.; Garcia, R.; Warrender, S. J.; Slawin, A. M. Z.; Wright, P. A.; Cox, P. A.; Fecant, C.; Mellot-Dranznieksd, C.; Bats, N. *Chem. Commun.* **2007**, 3470−3472. (b) Tzoulaki, D.; Heinke, L.; Castro, M.; Cubillas, P.; Anderson, M. W.; Zhou, W.; Wright, P.; Kärger, J. *J. Am. Chem. Soc.* **2010**, *132*, 11665−11670.
(17) Zhdanov, S. P.; Khvostchov, S. S.; Feoktistova, N. N. *Synthetic Zeolites*; Gordon and Breach: New York, 1990.
(18) Breck, D. W. *Zeolite Molecular Sieves*; John Wiley & Sons: New York, 1974.
(19) Corma, A.; Rey, F.; Rius, J.; Sabater, M. J.; Valencia, S. *Nature* **2004**, *431*, 287−290.
(20) Sierra, L.; Deroche, C.; Gies, H.; Guth, J. L. *Microporous Mater.* **1994**, *3*, 29−38.
(21) (a) Huang, A.; Caro, J. *Microporous Mesoporous Mater.* **2010**, *129*, 90−99. (b) Huang, A.; Liang, F.; Steinbach, F.; Gesing, T. M.; Caro, J. *J. Am. Chem. Soc.* **210**, *132*, 2140−2141. (c) Schreyeck, L.; D'agosto, F.; Stumbe, J.; Caullet, P.; Mougenel, J. C. *Chem. Commun.* **1997**, *13*, 1241−1242.
(22) Baerlocher, C.; McCusker, L. B.; Olson, D. H. *Atlas of Zeolite Framework Types*; Elsevier: Amsterdam, 2007.
(23) Chmelik, C.; Heinke, L.; Valiullin, R.; Kärger, J. *Chem. Ing. Tech.* **2010**, *82*, 779−804.
(24) Crank, J. *The Mathematics of Diffusion*; Clarendon Press: Oxford, 1975.
(25) Lehmann, E.; Chmelik, C.; Scheidt, H.; Vasenkov, S.; Staudte, B.; Kärger, J.; Kremer, F.; Zadrozna, G.; Kornatowski, J. *J. Am. Chem. Soc.* **2002**, *124*, 8690−8692.
(26) Lee, L. K.; Ruthven, D. M. *J. Chem. Soc., Faraday Trans. 1* **1979**, *75*, 2406−2422.
(27) Heinke, L.; Chmelik, C.; Kortunov, P.; Shah, D. B.; Brandani, S.; Ruthven, D. M.; Kärger, J. *Microporous Mesoporous Mater.* **2007**, *104*, 18−25.
(28) (a) Hausser, K. H.; Kalbitzer, H. R. *NMR in Medicine and Biology*; Springer: Berlin/Heidelberg/New York, 1991. (b) Vlaardingerbroek, M. T.; den Boer, J. A. *Magnetic Resonance Imaging: Theory and Practice*; Springer: Berlin/Heidelberg/New York, 2004.
(29) (a) Blümich, B. *Essential NMR*; Springer: Berlin/Heidelberg, 2005. (b) Kimmich, R. *NMR Tomography, Diffusometry, Relaxometry*; Springer: Berlin, 1997.
(30) Krishna, R. *J. Phys. Chem. C.* **2009**, *113*, 19756−19781.
(31) Ruthven, D. M. In *Adsorption and Diffusion*; Karge, H. G., Weitkamp, J., Eds.; Springer: Berlin/Heidelberg, 2008; Vol. 7, pp 1−43.
(32) Krishna, R.; van Baten, J. M. *Microporous Mesoporous Mater.* **2008**, *109*, 91−108.
(33) Bux, H.; Liang, F.; Li, Y.; Cravillon, J.; Wiebcke, M.; Caro, J. *J. Am. Chem. Soc.* **2009**, *131*, 16000−16001.
(34) Schemmert, U.; Kärger, J.; Krause, C.; Rakoczy, R. A.; Weitkamp, J. *Europhys. Lett.* **1999**, *46*, 204−210.
(35) Hibbe, F.; Chmelik, C.; Heinke, L.; Li, J.; Ruthven, D. M.; Tzoulaki, D.; Kärger, J. *J. Am. Chem. Soc.* **2011**, *133*, 2804−2807.
(36) (a) Heinke, L.; Kärger, J. *Phys. Rev. Lett.* **2011**, *106*, 74501. (b) Sholl, D. S. *Nature Chem.* **2011**, *3*, 429−430.
(37) Pan, L.; Parker, B.; Huang, X.; Olson, D.; Lee, J.-Y.; Li, J. *J. Am. Chem. Soc.* **2006**, *128*, 4180−4181.
(38) Dudko, O. K.; Berezhkovskii, A. M.; Weiss, G. H. *J. Chem. Phys.* **2004**, *121*, 11283−11288.
(39) Tuck, C. *Effective MediumTtheory*; Oxford University Press: Oxford, 1999.
(40) Barrer, R. M. *Zeolites and Clay Minerals as Sorbents and Molecular Sieves*; Academic Press: London, 1978.
(41) Kärger, J. *AIChE J.* **1982**, *28*, 417−423.
(42) Heinke, L.; Kortunov, P.; Tzoulaki, D.; Kärger, J. *Adsorption* **2007**, *13*, 215−223.
(43) Kirchner, T. Diffusion as a Probe of Structural Properties of Porous Solids. Diploma Thesis, Leipzig University, 2010.
(44) Hedin, N.; DeMartin, G. J.; Strohmaier, K. G.; Reyes, S. C. *Microporous Mesoporous Mater.* **2007**, *98*, 182−188.
(45) Hedin, N.; DeMartin, G. J.; Roth, W. J.; Strohmaier, K. G.; Reyes, S. C. *Microporous Mesoporous Mater.* **2008**, *109*, 327−334.
(46) Ruthven, D. M.; Reyes, S. C. *Microporous Mesoporous Mater.* **2007**, *104*, 59−66.
(47) Brandani, S.; Hufton, J.; Ruthven, D. *Zeolites* **1995**, *15*, 624−631.
(48) (a) Olson, D. H.; Camblor, M. A.; Villaescusa, L. A.; Kühl, G. H. *Microporous Mesoporous Mater.* **2004**, *67*, 27−33. (b) Jee, S.; Sholl, D. S. *J. Am. Chem. Soc.* **2009**, *131*, 7896−7904. (c) Vidoni, A. Ph.D. Thesis, University of Maine, 2011.

(49) Heink, W.; Kärger, J.; Pfeifer, H.; Datema, K. P.; Nowak, A. K. *J. Chem. Soc., Faraday Trans.* **1992**, *88*, 3505−3509.
(50) Jobic, H.; Kärger, J.; Krause, C.; Brandani, S.; Gunadi, A.; Methivier, A.; Ehlers, G.; Farago, B.; Haeussler, W.; Ruthven, D. M. *Adsorption* **2005**, *11*, 403−407.
(51) Heink, W.; Kärger, J.; Ernst, S.; Weitkamp, J. *Zeolites* **1994**, *14*, 320−325.
(52) Corma, A.; Kärger, J.; Krause, C. *Diffusion Fundam.* **2005**, *2*, 87.
(53) Kärger, J. *Microporous Mesoporous Mater.* **2008**, *116*, 715−717.
(54) (a) Vasenkov, S.; Kärger, J. *Microporous Mesoporous Mater.* **2002**, *55*, 139−145. (b) Feldhoff, A.; Caro, J.; Jobic, H.; Krause, C. B.; Galvosas, P.; Kärger, J. *Chem. Phys. Chem.* **2009**, *10*, 2429−2433.
(55) Schüring, A.; Auerbach, S. M.; Fritzsche, S.; Haberlandt, R. *J. Chem. Phys.* **2002**, *116*, 10890−10894.
(56) (a) Breck, D. W.; Eversole, W. G.; Milton, R. M.; Reed, T. B.; Thomas, T. L. *J. Am. Chem. Soc.* **1956**, *78*, 5963. (b) Reed, T. B.; Breck, D. W. *J. Am. Chem. Soc.* **1956**, *78*, 5972.